



Synergistic effects of soil microstructure and bacterial EPS on drying rate in emulated soil micromodels



Jinzi Deng ^{a,1}, Erika P. Orner ^{a,1}, Jessica Furrer Chau ^b, Emily M. Anderson ^a,
 Andrea L. Kadilak ^a, Rebecca L. Rubinstein ^c, Grant M. Bouchillon ^c, Reed A. Goodwin ^d,
 Daniel J. Gage ^d, Leslie M. Shor ^{a,e,*}

^a Department of Chemical and Biomolecular Engineering, University of Connecticut, Storrs, CT, USA

^b Department of Physics and Engineering, Benedict College, Columbia, SC, USA

^c Department of Civil and Environmental Engineering, University of Connecticut, Storrs, CT, USA

^d Department of Molecular and Cellular Biology, University of Connecticut, Storrs, CT, USA

^e Center for Environmental Sciences & Engineering, University of Connecticut, Storrs, CT, USA

ARTICLE INFO

Article history:

Received 21 April 2014

Received in revised form

4 November 2014

Accepted 14 December 2014

Available online 26 December 2014

Keywords:

Extracellular polymeric substances (EPS)

Microdevice

Microfluidic device

Pore-scale

Sinorhizobium meliloti

Soil moisture

ABSTRACT

Microbial extracellular polymeric substances (EPS) have been shown to alter soil moisture retention and to improve seedling survival and plant growth at the bulk scale. The mechanisms of EPS-mediated water retention include reversible swelling of the cross-linked polymer matrix and the promotion of an aggregated soil structure. However, the effects of EPS on water retention have never been directly observed at the pore scale. Here, emulated soil micromodels were developed to directly observe the effects of physical, chemical, and biological factors on pore-scale water retention. In this demonstration, a pseudo-2D pore structure was created to represent physical features of a fine sandy loam. Replicate micromodels were initially saturated with suspensions of different soil bacteria, and pore-scale air infiltration was directly imaged over time. External evaporativity was held constant through the use of a custom constant-humidity environmental chamber. Micromodels filled with suspensions of highly mucoid *Sinorhizobium meliloti* retained moisture about twice as long as physically identical micromodels filled with suspensions of non-mucoid *S. meliloti*. Relative drying rates in six replicate experiments ranged from 1.1 to 2.5 times slower for mucoid suspensions. Patterns of air infiltration were similar but not identical across replicates. The results suggest that pore fluid EPS and micromodel geometry act together to limit evaporation at pore throats. Advantages of the micromodel approach include direct observation of pore-scale dynamic process, and the ability to systematically replicate complex physical structures. These abilities will enable users to screen benefits from different structures and from microbial compositions, and build predictive understanding of the overall function of microbe-habitat systems.

© 2014 Elsevier Ltd. All rights reserved.

* Corresponding author. Department of Chemical and Biomolecular Engineering, University of Connecticut, 191 Auditorium Rd. Unit 3222, Storrs, CT 06269-3222, USA. Tel.: +1 860 4863136.

E-mail addresses: jinzi.deng@gmail.com (J. Deng), Erika.p.ornier@gmail.com (E.P. Orner), chauj@benedict.edu (J.F. Chau), ee905@yahoo.com (E.M. Anderson), Andrea.Kadilak@uconn.edu (A.L. Kadilak), Rebecca.L.Rubinstein@uconn.edu (R.L. Rubinstein), gbouchillon@gmail.com (G.M. Bouchillon), reed.goodwin@uconn.edu (R.A. Goodwin), Daniel.Gage@uconn.edu (D.J. Gage), LeslieShor@gmail.com (L.M. Shor).

¹ These authors contribute equally.

1. Introduction

Global climate change is predicted to amplify extreme events in the water cycle, leading to widespread reduction in soil moisture (Dai, 2011), with important implications for sustainable food, feed, and fiber production. Following a rain event, water is lost from the soil by infiltration and evaporation. The rate of evaporation is dependent on a host of factors including meteorological conditions, land use, and depth of the water table. Other important factors include micro-scale variations in soil characteristics such as soil texture, structure, and organic matter content, and the activities of plants and soil microbes.

As reviewed recently, soil moisture is a key factor influencing microbial respiration (Moyano et al., 2013). In turn, microbial processes modulate water availability in soil through production of extracellular polymeric substance (EPS) (Or et al., 2007a). Roberson and Firestone (1992) showed dramatic shifts in water retention in porous media amended with small amounts of hydrogel, and these authors speculated that bacterial control of the microenvironment could enhance their survival. Since then, the concept of soil as a self-organizing physical-biological system has emerged (Young and Crawford, 2004).

In soils, the vast majority of bacteria are found in biofilms, where bacteria embedded in EPS are better protected from changing soil water conditions (Or et al., 2007a) and predation (Matz and Kjelleberg, 2005) and enjoy greater access to water-soluble nutrients (Chenu and Roberson, 1996). Microbial biofilms are comprised of one or several species of bacteria embedded in an EPS matrix of proteins, polysaccharides and DNA. EPS has a highly cross-linked structure that enables it to shrink and swell yet remain saturated across a wide range of matric potentials (Or et al., 2007a). The micro-scale structure of biofilms includes several layers of bacteria, each with different phenotypes (Ramos et al., 2001; Sauer et al., 2002), and pores and networks facilitating the flow of nutrients and oxygen (Li and Yuan, 2002).

In a soil system, EPS acts with mineral grains and plants to retain and direct moisture. Mucoid bacteria may contribute to soil structuring (Alami et al., 2000). Production of EPS promotes both the formation (Amellal et al., 1998; Gajic et al., 2010) and the stability (Park et al., 2007) of soil aggregates. Soil aggregates tightly hold moisture in interstitial spaces (Or et al., 2007b) while larger inter-aggregate spaces promote drainage and gas exchange (Morales et al., 2010). Aggregated soils thus tend to sustain the intermediate water contents that are most favorable to plants and soil microbes (Kets et al., 1996). In the rhizosphere, EPS is predicted to act as both a reservoir and a conductor of water to plant roots when bulk soil water is scarce (Carminati et al., 2011).

Prior research has measured the effect of EPS on survival and growth of plants, but only at the bulk scale. For example, Sandhya et al. (2009) showed that inoculation with EPS-producing *Pseudomonas* sp. strain GAP-P45 increased sunflower seedling survival and plant biomass under water-stressed conditions. Similarly, Alami et al. (2000) showed that sunflower seed or soil inoculation with *Sinorhizobium* sp. strain YAS34 caused an increase in root-adhering soil per root dry mass of up to 100%. Root-adhering soil helped to counteract the deleterious effects of water deficit on growth and also promoted fertilizer uptake.

Only occasionally have interacting physical and biological processes been considered at the pore scale. For example, Dechesne et al. (Dechesne et al., 2010) and Wang and Or (Wang and Or, 2010) described cell migration and emergence of colony patterns based on spatial distribution of hydrated pore regions. Other researchers have employed agent-based microbial community models to demonstrate emergent functionality in micro-structured habitats (Long and Or, 2009; Wang and Or, 2013). These studies provide important insights into the interactions of microbes and micro-structured habitats. However, to date, the effect of bacterial EPS on pore-scale evaporation processes has never been determined in a physically micro-structured experimental setting.

Here, soil micromodels were developed to better understand pore-scale effects of bacterial EPS on drying resistance. Micromodels allow faithful replication of micrometer-scale physical and chemical features of microbial habitats, and enable direct observation of microbial responses (Weibel et al., 2007). Microfluidic devices have been used to study bacterial spatial coordination (Cho et al., 2007), the stability of microbial communities (Kim et al., 2008), bacterial chemotaxis (Mao et al., 2003; Lanning et al.,

2008; Long and Ford, 2009), bacteria-enhanced solute dispersion (Singh and Olson, 2011), and the mobility of protozoa in narrow channels (Wang et al., 2005, 2008). We know of no prior efforts to use microfluidic devices to measure drying resistance at the pore scale, or as a function of bacterial EPS.

The objective of this study was to visualize and measure the effects of bacterial EPS on evaporation of soil water at the pore scale, which is the physical scale most relevant to bacterial colonization and water retention processes. Our hypothesis is that EPS and soil microstructure act together to limit evaporation from soils. Soil micromodels were created to emulate the physical structure and pore geometry of a sandy loam, but in a pseudo-2D format to allow direct optical visualization of air infiltration into pores. By employing a microfluidic device with emulated soil structure, soil particle size and distribution as well as porosity can be exactly replicated in every experiment.

Here, emulated soil micromodels were colonized with mucoid (EPS+, a strain that produces well-characterized EPS) or non-mucoid (EPS-, a control strain that does not produce any EPS) *Sinorhizobium meliloti*. Air infiltration into the physically-identical micromodels was imaged over time in a constant-humidity chamber placed on an inverted microscope. The effects of EPS on changing water content were imaged directly within the micromodel. In addition, thermogravimetric analysis (TGA) was used to measure drying of *S. meliloti*-amended soil, and dynamic vapor sorption (DVS) was used to measure drying of bacterial colony samples of *S. meliloti*. By comparing the TGA results with the DVS results, we find additional support for the hypothesis that EPS and soil microstructure act synergistically to limit evaporation from soils. Finally, we propose a mechanism for the increased evaporation resistance observed in EPS+ trials in structured habitats.

2. Materials and methods

2.1. Bacterial strains

Drying experiments in soil micromodels and sterilized air-dried soil samples were performed with mucoid and non-mucoid strains of *S. meliloti*. *S. meliloti* and related bacteria are agriculturally and environmentally important as symbionts of legumes due to their nitrogen fixation abilities (Gage, 2004). The commonly used lab strain *S. meliloti* Rm1021 has been sequenced and studied extensively (Galibert et al., 2001; Pellock et al., 2002). Rm1021 is a quorum sensing mutant with a natural insertion in *expR* that results in relatively low level production of the exopolysaccharide galactoglucan (EPSII) (Pellock et al., 2002). Strain Rm8530, which lacks the insertion, is very mucoid due to the over-production of EPSII. In addition, regulation of EPSII by *expR* plays a key role in the ability of *S. meliloti* to form biofilms (Rinaudi and Gonzalez, 2009).

Here, we focus on strain Rm8530, designated here as “EPS+”, and compare it to *S. meliloti* strain Rm11609 (Rm1021 *exoY*, *expA*) as a “control strain” due to its inability to produce EPSI or EPSII (Mueller and Gonzalez, 2011). Strain Rm11609 is designated here as “EPS-” (Table 1).

Table 1
Characteristics of different strains of *Sinorhizobium meliloti*.

Strain	Characteristics	EPS characteristics
Rm8530	Rm1021 <i>expR</i> ⁺	EPS+
Rm11609	Rm8530 <i>exoY::OTC</i> ⁺ <i>expA::Nm</i> ⁺	EPS-

2.2. Microfluidic device concept

Soil micromodels were comprised of three rectangular channels connected to a single inlet well and a single outlet well (Fig. 1A). Each 20 mm × 1 mm × 0.034 mm rectangular channel contained a 10 mm-long microstructured region, with pillars of varying sizes and shapes representing a two-dimensional slice of the solid phase of a simulated sandy loam (Fig. 1B).

The geometry of the microstructured region was based on a realistic computer-generated three-dimensional packing of ellipsoidal particles into a computational domain of size 100 × 100 × 100 voxels. The size distribution of these particles was based on a truncated, experimentally-determined sandy loam particle size distribution (Chau et al., 2011). A scale of one lattice unit to 5 μm (that is, one voxel to (5 μm)³ = 125 μm³) was chosen based upon computational and microfluidic device fabrication constraints. Particle sizes were constructed using USDA size ranges (fine sand 125–250 μm, and very fine sand 50–125 μm). A set of particles in the two size fractions was generated randomly, with the particle number tuned to create the appropriate percentage of the total solid volume (56% fine sand, 44% very fine sand). Particles were generated as ellipsoids by drawing radii from a uniform distribution dictated by particle size, then randomly taking sets of three (r_x , r_y , and r_z) and keeping only sets conforming to sphericity values $0.7 \leq S = r_{\min}/r_{\max} \leq 0.85$, based on the properties of sand particles (Friedman and Robinson, 2002; Cho et al., 2006). Particles were then randomly placed in a three-dimensional computational domain, and a packing algorithm DigiPac (Jia and Williams, 2001) was employed to create realistic particle–particle contacts. Finally, a two-dimensional slice of the packed three-dimensional domain was selected with desired porosity and pore geometry.

The selected two-dimensional slice was converted to a two-toned bitmap. AutoCAD Raster Design 2010 was used to manually outline and vectorize the particle contours in the bitmap. The resulting structure was partitioned to completely fill the 1 mm × 10 mm microstructured region in a high-resolution chrome-on-glass photomask.

Particle diameters ranged from 10 to 300 μm with an average diameter of 110 μm while pore radii ranged from 16 to 130 μm with an average hydraulic radius of 44 μm (Fig. S1). Average particle diameters and pore radii (calculated as the hydraulic radius = 2 × area/perimeter) were obtained using image analysis of the original bitmap version of the micromodel design (Fig. 1B) in MATLAB (MathWorks, Natick, MA). Soil used for TGA was the corresponding 75–250 μm fraction sieved from whole soil. Typical porosities for a sandy loam are in the range of 25–35%. The porosity of our pseudo-2D soil chip was 57%. The higher porosity is expected

for a 2-D slice of packed 3-D model that maintains pore connectivity in 2-D (Chau et al., 2005; Chau and Or, 2006).

2.3. Micromodel fabrication

Physically identical soil micromodels were cast in polydimethylsiloxane (PDMS) from a microfluidic casting master. PDMS (Si(CH₃)₂–O–)_n is an inexpensive and biocompatible polymer that offers excellent optical clarity and readily conforms to micron-scale physical features (Whitesides et al., 2001). PDMS microfluidic devices have been used extensively for cell culture, especially for applications in the biomedical field. Upon exposure to oxygen plasma, PDMS surface charge is similar to quartz sand (Roman and Culbertson, 2006).

Microfluidic casting masters were created using photolithography, a commonly-used technique, as described in detail elsewhere (Markov et al., 2010; Deng et al., 2013). Briefly, a thin layer of SU-8 2025 photoresist (Microchem, Newton, MA) was coated on a 4-inch diameter Si wafer (Nova Electronic Materials, test grade, Flower Mound, TX). The thickness of the photoresist coating was 34 ± 3 μm as determined by profilometry (Dektakmodel 150, VeecoInstruments, Plainview, NY). The photoresist was photopatterned using a chrome-on-glass photolithography mask (Advanced Reproductions, North Andover, MA) with 26.4 mW cm⁻² ultraviolet light for 6.1 s (OAI 200 mask aligner, San Jose, CA) followed by cross-linking and developing steps.

Finished masters were silanized to facilitate repeated PDMS casting based on methods described previously (Addae-Mensah et al., 2009; Langelier et al., 2011). Briefly, the master was cleaned with isopropanol (Laboratory Grade, Fisher Chemical, Pittsburgh, PA) and dried with N₂ (Industrial Grade, Airgas, Waterford, CT). To evenly oxidize the surface, the master was treated with O₂ plasma (300 W, 4 min) using a Microwave Plasma System (PS 210, PVA TePla America, Inc., Corona, CA). The plasma-treated master was positioned SU-8-side down on a disposable aluminum weight dish containing 3–5 drops of the silanizing agent (tridecafluoro-1,1,2,2-tetrahydrooctyl)trichlorosilane (UCT, Inc., Bristol, PA). The dish and master were placed inside a vacuum desiccator, and the silane was evaporated and deposited on the surface of the master under –75 kPa gage vacuum for 1 h. Finally, any remaining silane was volatilized by heating the master uncovered on a hot plate at 150 °C for 10 min.

Emulated soil micromodels were cast 1 cm thick in PDMS (Sylgard 184, Dow Corning, Midland, MI). Briefly, PDMS base and curing agent were fully mixed in a 10:1 ratio then degassed at –75 kPa gage for 30 min, poured over the master, and cured in an oven at 60 °C for 4 h. Once cured, castings were carefully peeled

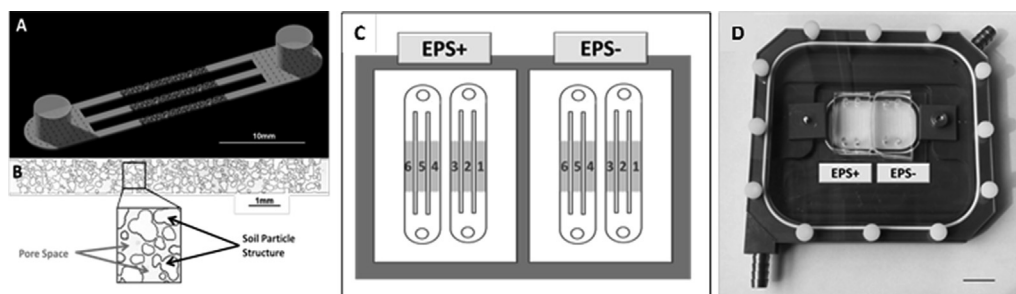


Fig. 1. Schematic of the emulated soil micromodel design. (A) Rendering of the emulated soil micromodel with 3 identical channels, each with a micro-structured region 10 mm long, 1 mm wide, and 34 ± 3 μm-deep. Access ports were 1 cm high and 4 mm in diameter. (B) Tiled micrograph of the 2-D pore structure used in every micromodel (9 tiled micrographs, scale = 1 mm). Features labeled “soil particles” are columns of uniform size in the z-direction (i.e., out of the plane). (C) Schematic of drying experiments: replicate soil micromodels each comprised of three identical micro-structured drying channels were loaded with suspensions of mucooid (EPS+) or non-mucooid (EPS–) *S. meliloti* bacteria suspended in artificial groundwater. (D) Photograph of micromodels installed in the custom-built environmental control chamber (scale = 2 cm).

from the master, trimmed, and access ports were manually punched from the patterned side using a 4 mm biopsy punch (Miltex, Inc., York, PA). Each casting was treated with O₂ plasma for 45 s in an evacuated air atmosphere (Harrick PDC-32G, Harrick Plasma, Ithaca, NY) then aligned and irreversibly bonded to a plasma-treated (45 s) glass microscope slide in the arrangement shown in Fig. 1C and D.

2.4. Micromodel operation

Once bonded, micromodels were filled with suspensions of bacteria and were considered 100% saturated. Each bacterial strain was cultured for 5 d at 30 °C and 100 rpm in covered 20 ml Pyrex Vista rimless culture tubes (Corning, Tewksbury, MA) in M9 minimal medium also containing 0.4% glycerol, 500 µg ml⁻¹ streptomycin, and 100 µg ml⁻¹ spectinomycin. For *S. meliloti* Rm11609, the medium also contained 100 µg ml⁻¹ neomycin and 0.75 µg ml⁻¹ oxytetracycline. Stationary phase cultures were washed three times in artificial groundwater (AGW) (Scholl et al., 1990) containing 0.100 mM KH₂PO₄ then adjusted to OD₅₉₅ 0.012 for *S. meliloti* Rm8530 or OD₅₉₅ 0.010 for *S. meliloti* Rm11609 to obtain comparable cell concentrations of 10⁷ cells ml⁻¹.

Plasma-treated PDMS has a hydrophilic surface chemistry and can be readily filled with aqueous solutions using capillarity (Bouchillon et al., 2014). Four replicate micromodels were filled with AGW suspensions of bacteria: two with *S. meliloti* Rm8530 (EPS+) and two with *S. meliloti* Rm11609 (EPS-) (Fig. 1C). Then, all micromodels were held for a 5 d conditioning period at ambient temperature (approx. 23 °C) and 100% relative humidity. This conditioning period allowed the bacterial community to stabilize biomass, EPS, and aggregation state, and also allowed the PDMS polymer to saturate with water.

2.5. Design and operation of environmental control chamber

A custom-built environmental control chamber was used to hold the external evaporativity constant during prolonged drying experiments, even if the micromodel was temporarily removed from the microscope stage. The design of the chamber was adapted from Steinhaus et al. (Steinhaus et al., 2007). As implemented here, the control chamber fit between the stage and condenser of an AxioObserver Z1 AX10 inverted wide field microscope (Carl Zeiss, Oberkochen, Germany), and was securely installed recessed into a Märzhäuser programmable scanning stage. (Additional technical details of the design are available in supplementary information, Figs. S2 and S3).

After the 5 d conditioning period, micromodels were installed in the environmental control chamber over the open viewing window (Fig. 1D) and the clear polycarbonate lid was secured. Metal barbed tube fittings at two corners allowed humidity-controlled air to continuously circulate through the environmental chamber. Humidified air was created in a separate 0.5 m³ mixing chamber containing a Cigar Oasis XL humidifier (Orlando, FL) set to 80% relative humidity, corresponding to -30 MPa (matric potential value). An HT10 USB Humidity Temperature Data Logger (General Tools, New York, NY) placed in the microscope-mounted chamber continuously recorded humidity (78% ± 2%) and temperature (19°C ± 0.5 °C) during the experiment.

2.6. Imaging and image analysis

The progression of the air–water interface was determined throughout all 12 microchannels every 30 min from the time when the air interface was at the edge of the microstructured region until air had fully infiltrated. Bright-field composite images were

captured using a Carl Zeiss AxioObserver Z1 AX10 automated inverted microscope equipped with an AxioCam MRmRev.3 camera using a 5× objective (Zeiss EC Plan-Neofluar; 5 × /0,16 ∞/0,17). Composite images were constructed by stitching together 9 overlapping frames using the AxioVision 4.8 software (see e.g. Fig. 1B).

Composite images were analyzed using the open-source Fiji image-processing package (Schindelin et al., 2012). First, each composite image was cropped and then converted to a binary, black and white image. Using a single threshold value, a continuous air interface along hydrated pore space or PDMS pillars could be resolved in all composite images. Next, the continuous air phase was manually filled with black pixels using the position of the air interface as a guide (Fig. 2). Total “air” pixels at each time point in each composite image were quantified in Fiji then converted to an air volume (mm³) using a uniform channel height of 34 µm. Finally, the air volume was subtracted from the known total pore volume to determine the remaining water volume and the relative water saturation.

2.7. Thermogravimetric analysis

As a qualitative support of the results obtained using soil micromodels, evaporation kinetics of water from a sandy loam soil amended with EPS+ or EPS- bacterial suspensions were measured using thermogravimetric analysis (TGA). TGA involves gravimetric determination of mass loss from a sample over time as a result of a pre-determined temperature cycle. Bacterial-amended soils were first subjected to a period of desiccation and rewetting prior to TGA in order to better simulate the variable environmental conditions to which soil microbes are acclimated.

Paxton and Montauk fine sandy loam was collected from the Horsebarn Hill area of the University of Connecticut Storrs campus. Whole soil was screened in the field, autoclaved, air dried, and sieved to obtain the 75–250 µm fraction, corresponding to the particle size distribution of the soil micromodel (Fig. 1B and Fig. S1). Stationary-phase AGW suspensions of *S. meliloti* Rm8530 or Rm11609 at 10⁷ cells ml⁻¹ were prepared as described above. Excess volumes (5 ml) of bacterial AGW suspensions were added to

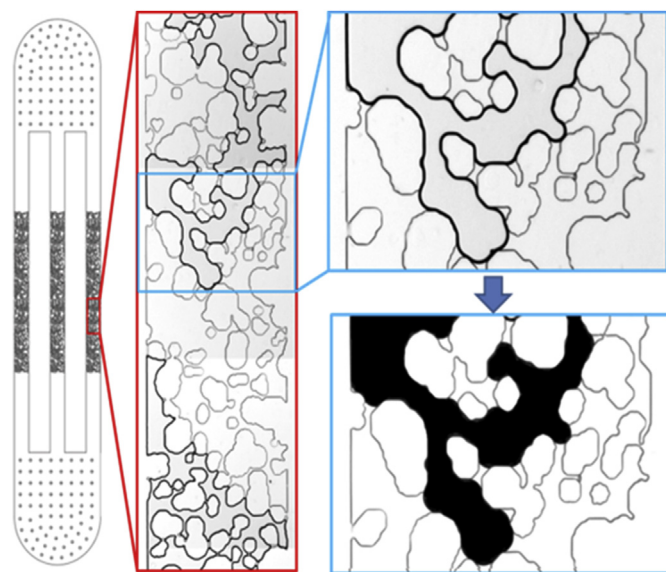


Fig. 2. Schematic showing image processing scheme: the position of the air–water interface was identified by applying a binary threshold super-imposed over the tiled image, then the invading air phase was manually converted to black for visual inspection and subsequent quantitative image processing.

1 g sterile, air-dry soil in 50 ml centrifuge tube (Corning, Tewksbury, MA), then slurries were covered and allowed to sit at ambient temperature (approx. 23 °C) for 5 d. Slurries were dried at 60 °C for 2 d, then 100 ± 1 mg dry bacteria-amended soil was loaded onto a tared hanging weigh pan. Dry bacteria-amended soil was re-hydrated by adding 40 μ L of AGW, and equilibrated at 23 °C at 100% relative humidity for 2 h prior to re-drying.

Tared, re-wetted, and equilibrated EPS+ or EPS- *S. meliloti*-amended soil samples were placed on a TGA (Q500, TA Instruments, New Castle, DE), and the change in weight was determined with time as heated dry air flowed past the sample. Samples were dried at 40 °C for 700 min to estimate labile water under environmental conditions, then dried at 105 °C for 120 min to determine total water. Finally, samples were oxidized at 360 °C for 120 min to determine the total organic carbon content (Schulte and Hopkins, 1996).

2.8. Dynamic vapor sorption

Dynamic Vapor Sorption (Q5000, TA Instruments, New Castle, DE) was used to measure the kinetics of water loss (evaporation) in pure bacterial colony samples collected from confluent bacterial lawns grown on agar plates. Liquid-phase *S. meliloti* Rm8530 (EPS+) and Rm11609 (EPS-) cultures were prepared as described above. Then, 300 μ l aliquots of stationary-phase culture were added to M9 agar plates with 0.4% glycerol, spread by shaking with 3 mm sterile glass beads, then incubated at 30 °C for 3 d. Colony samples (approx. 10 mg) were carefully scraped from the plates (taking care not to remove any agar) and placed into tared metalized quartz sample pans (TA Instruments, New Castle, DE).

Because initial water content in bacterial colony samples may vary between replicates due to humidity and temperature conditions on the day of experiments, colony samples were first dried to a consistent, low water content at 40 °C and 10% relative humidity

in N₂ for 9 h. Then, the humidity was increased to 90% in 10 min, and held steady for 9 h to allow biological material to rehydrate and swell with water vapor. Finally, for comparison with micromodel experiments, the humidity was decreased from 90% to 80% and the evaporation rate of water was determined gravimetrically.

3. Results

3.1. Pore-scale patterns of air infiltration

Composite images of microchannels depict the micro-scale progression of the air interface during drying. A down-selected time series of composite images is provided in Fig. 3. Across treatments and replicates, micro-structured features of the pore geometry constrained the progression of the air interface. For both EPS+ and EPS- treatments, air was observed to initially infiltrate more readily from the left side of each microchannel due to the random arrangement of pore throat sizes at the channel edges. Pore throat geometry also determined the advancement of the air-infiltration front, but the rate of advancement was different for EPS+ and EPS- replicates. In all replicates of both treatments, the air interface at the right remained fixed in either of two positions over several hours. For example, in channel 2 of the EPS- treatment, the air interface in the second composite image (after 2.5 h drying) was located about 8% across the channel, or about 1.6 mm from the right side (Fig. 3), with similar results for channels 3, 4, and 5. In the EPS+ treatment, the air interface also stalled at a similar position in channels 1, 3, 4, 5, and 6. However, the interface remained in this position much longer in the EPS+ treatments, up to 16.5 h. A second stall position can be seen in several channels, for example, in the 3rd-5th frames for channel 2 of the EPS+ treatment (Fig. 3). This second stall position was also observed in the other 5 channels of the EPS+ treatment, but for shorter durations (typically

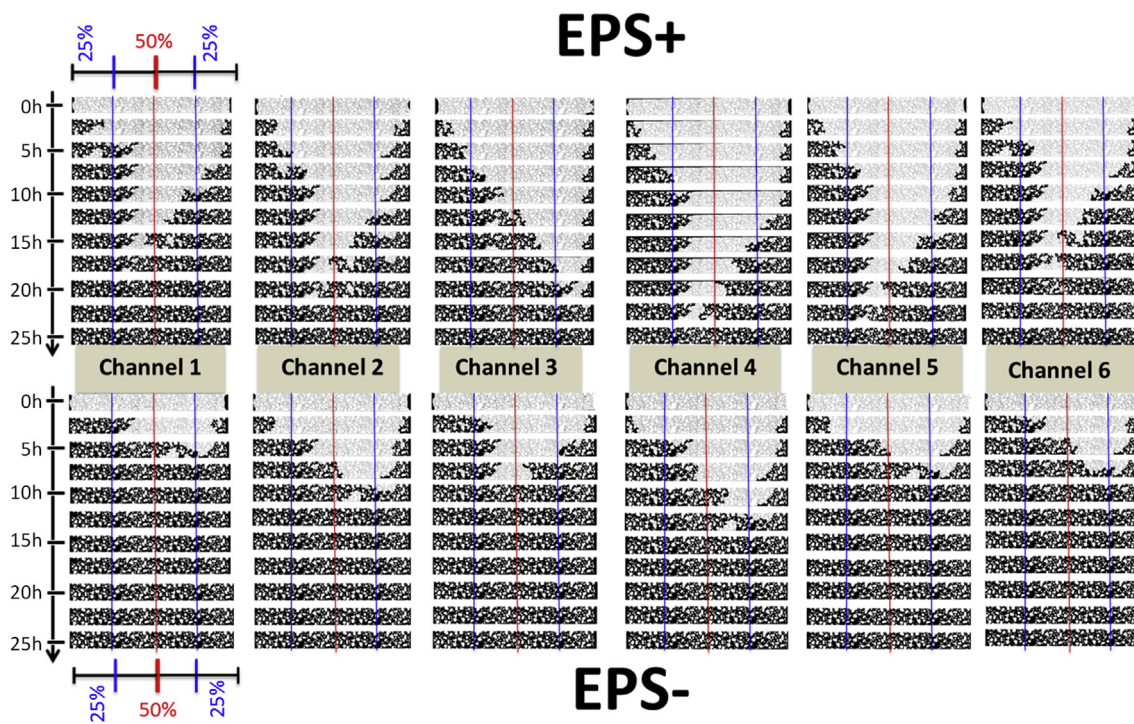


Fig. 3. Time series of composite images showing air infiltration (in black) in replicate microchannels. The time between frames is 2.5 h. Physically identical channels filled with EPS+ suspensions are at the top and channels filled with EPS- suspensions are at the bottom. The position of replicate channels in the control chamber is provided in Fig. 1C. Vertical lines signify the midline and the quartile distances from each edge of the 10 mm-long micro-structured region.

0.5 h). This second stall position was apparent in all of the channels of the EPS⁻ treatment for durations ranging from 2 to 5 h.

Across several of the channels, similar pore-scale patterns of air infiltration led to the persistence of hydrated pockets in certain regions separated from the rest of the pore network by narrow pore throats. One such region can be seen in Fig. 3, channel 1 of the EPS⁻ treatment, frame 3, about 33% along the channel from the right side. This hydrated pocket persists longer in the EPS⁺ treatment than in the EPS⁻ treatment. For example, it is observed in channel 1 and channel 6 of the EPS⁺ treatment for 5 frames each (2 h). The pocket is also observed in channels 1, 2, 4, and 5 of the EPS⁻ treatment, but only for an average of 1 h. Smaller hydrated pockets are also apparent in interstitial spaces between particles. Fig. 4 employs a chromatic time scale to map persistence of hydration within a sub-section of the microchannel. In the EPS⁺ treatment, several small spaces measuring just a few microns remain hydrated for up to 5 h (indicated by the dark green color). These same positions remained hydrated for 3 h in the EPS⁻ treatment.

3.2. Drying rates in micromodels containing EPS⁺ and EPS⁻ suspension

Soil micromodels loaded with EPS⁺ *S. meliloti* suspensions retained moisture longer than micromodels loaded with EPS⁻ *S. meliloti* suspension (Fig. 5A). On average, *S. meliloti* Rm11609 (EPS⁻) dried in 12.1 h with a standard deviation of 2.9 h, and Rm8530 (EPS⁺) dried in 22.7 h with a standard deviation of 3.1 h (Table 2). The drying rate for channels filled with the EPS⁻ suspension (Fig. 5B) decreased continuously, from around $0.3 \mu\text{g min}^{-1}$ at the beginning of the experiment to 0 within 18 h. The drying rate for channels in the EPS⁺ treatment was more consistent over time: generally water was lost at a rate of $0.15 \mu\text{g min}^{-1}$ for the first several hours and then the rate decreased gradually.

At 11 h into the drying process, average drying rates measured for the two treatments were similar ($0.16 \mu\text{g min}^{-1}$). At 11 h, microchannels filled with the EPS⁻ suspension were just 10% saturated, while microchannels filled with the EPS⁺ suspension were about 45% saturated. Towards the end of the drying process, the drying rate was greater in the EPS⁺ treatment channels (which

still had much more water to lose) than the nearly-desiccated microchannels of the EPS⁻ treatment.

Microchannels filled with EPS⁺ bacterial suspensions required more time to dry to a given relative saturation compared with microchannels filled with EPS⁻ bacterial suspensions (Fig. S4). EPS⁺ treatment microchannels required $4.5 \text{ h} \pm 1.4 \text{ h}$ (average \pm standard deviation) to reach 80% saturation versus $2.8 \pm 1.1 \text{ h}$ for EPS⁻ treatment microchannels. The EPS⁻ treatment channels dried to 80% saturation $1.6 \times$ faster than the EPS⁺ treatment microchannels. Similarly, the time required to reach other milestones of 60%, 40%, 20%, and 0% relative water saturation were significantly shorter for EPS⁻ treatment channels. The ratio of drying time in EPS⁻ to EPS⁺ treatments for these milestones was a factor of 2.0, 1.9, 1.9, and 1.9 times faster, respectively.

3.3. Thermogravimetric analysis of bacteria-amended soil

Labile water loss from rewetted bacteria-amended soil was determined in duplicate for each bacterial strain treatment. Water evaporation with drying (40 °C) was normalized to the last 3 mg of water remaining in 100 mg soil (Fig. S5A). No obvious difference in drying rate was observed between EPS⁻ amended soil and EPS⁺ amended soil in the early stages of drying (Fig. S5A). However, considering the last 3 mg water (7.5%), the normalized water content in EPS⁻ amended soil was lower than the water content in EPS⁺ amended soil ($p < 0.0001$) (Fig. S5B).

3.4. Dynamic vapor sorption analysis of bacterial colony samples

Bacterial EPS can retain moisture in soil two ways: by holding water directly in the cross-linked hydrogel polymer itself, and through soil structuring which alters the physical arrangement of soil grains. Here, to understand the ability of EPS to hold water directly without a physical structure, the swelling and drying behavior of duplicate bacterial colony samples collected from agar plates for both model strains was analyzed using dynamic vapor sorption.

The weight of each bacterial colony sample was normalized to its weight at equilibrium in 90% relative humidity. Then, once humidity was reduced to 80%, the loss of weight with evaporation was measured over time (Fig. S6A and B). The data show there is no difference in water content of bacterial colony samples of EPS⁺ versus EPS⁻ strains.

4. Discussion

4.1. Pore-scale mechanisms of water retention and evaporation

The rate of air infiltration into replicate emulated soil micromodels depends on the combined effects of the physical features of the microstructure and the chemical composition of the interstitial fluid. Progression of the air–water interface through the pore spaces in microchannels is determined by the evaporative flux of water across the air–water interface and diffusion of water vapor along the air-filled microchannel. The evaporative flux depends on the relative magnitude of the matric and solute potential of the wetting phase (EPS solution) and the lower potential of water vapor in the air phase.

In our micromodel experiments, all replicates were subject to identical, constant relative humidity and temperature boundary conditions, thus determining the potential of the water vapor according to $R_H = \exp((MW_w \psi_w)/(\rho_w RT))$ (Or and Wraith, 2002) where MW_w is the molecular weight of water, ψ_w is water potential, ρ_w is water density, R is the universal gas constant, and T is absolute temperature. The 80% relative humidity applied external to the soil

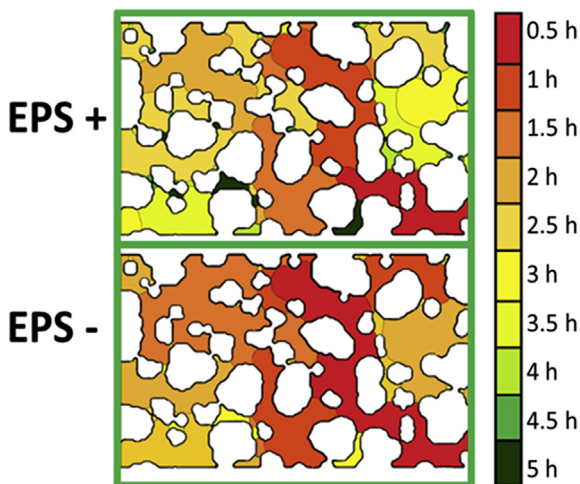


Fig. 4. Chromatic illustration of air infiltration with time: air infiltration that occurs in the first 0.5 h is represented in red, and infiltration at each subsequent 0.5 h period is represented by the chromatic series through green at 5 h. Note the propensity for the air–water interface to exist at pore throats, and the persistence of hydrated pockets in the EPS⁺ treatment.

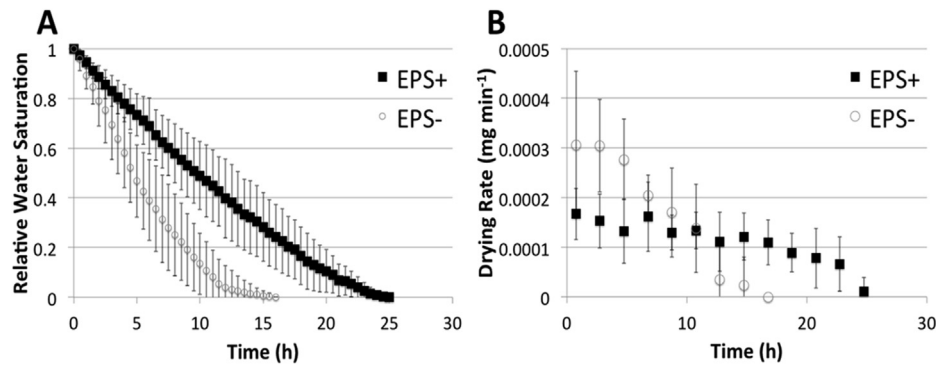


Fig. 5. (A) Relative water saturation versus time for channels filled with EPS+ or EPS- bacterial suspensions (average and standard deviation of 6 replicates). (B) Instantaneous drying rate using a 2 h moving average (average and standard deviation of 6 replicates).

micromodel corresponds to a matric potential of -30 MPa, representing extremely dry conditions under which bacterial respiration would cease in a real soil (Potts, 1994; Or et al., 2007a). This condition was chosen to produce reasonable drying times for the micromodels under EPS+ and EPS- conditions.

Because the physical geometry is identical, the diffusivity of water vapor away from the air–water interface is also identical between replicate channels. The potential of liquid water is a function of the physical geometry of the microchannel and the chemical composition of the EPS solution. Physical geometry varies with position, and chemical composition may vary with both position and time due to the dynamic activities of live bacteria.

The physical geometry of the micromodels determines the path taken by the invading air phase. Air invasion into a porous medium exhibits invasion-percolation behavior (Sukop and Or, 2003) in which the non-wetting fluid (air) first invades the largest pore throat where capillary forces are weakest. Once the throat is breached, the comparatively large pore space behind it fills with air quickly (i.e., the water evaporates), followed by the next-largest pore throat of the new interfacial configuration.

Here, air infiltration behavior is consistent with invasion-percolation behavior. The path taken by the air interface was observed to follow similar patterns across treatments and replicates. Certain regions in the microchannels readily admitted the invading air space, while others regions with narrow pore throats were associated with stall positions of the air interface, or boundaries of persistent hydrated pockets. As in natural porous media, water is held more strongly in narrow hydrophilic spaces between PDMS pillars where capillarity is strongest. As stated earlier, PMDS exhibits a hydrophilic surface chemistry after exposure to oxygen plasma, with a surface charge similar to quartz sand (Roman and Culbertson, 2006). Also, the surface chemistry of PMDS remains hydrophilic as long as water is in contact with PDMS (Mukhopadhyay, 2007).

Microfabrication conserves the physical geometry across treatments and replicates, resulting in reproducible patterns of air

infiltration. However, live bacteria move, grow, and respire within the microchannels. The resulting spatial distribution and population density of microbial communities and the chemical composition of the interstitial fluid after the 5 d conditioning period may vary between replicates, and especially if bacteria have aggregated at critical pore throats. The variable behavior of the bacterial population may have been responsible for the variations observed in patterns of air infiltration across replicates.

The chemical composition of the interstitial fluid also affects the rate of evaporation from microchannels. Here, fluid in the pore spaces contains a mixture of bacterial cells, salts, proteins, small molecules, and especially in the EPS+ treatment, extracellular polymers. Hydrogels are known to retain moisture through the favorable entropy of mixing between H₂O molecules and the polysaccharide, resulting in a lower activity of water in the hydrogel phase relative to pure water phase (Flemming, 2011).

Here we show, for both whole soils and soil micromodels, amendment with the EPS+ strain resulted in a marked evaporation resistance. The evaporation time ranged from 1.1 to $2.5 \times$ slower in replicate micromodels, with an average of $1.9 \times$ slower for EPS+ versus EPS- treatments. In the corresponding size fraction of bacteria-amended soil, water content is also higher, but only when approaching dryness ($p < 0.0001$). In the micromodels, the surface area available for air infiltration are the $1 \text{ mm} \times 34 \text{ }\mu\text{m}$ openings at the ends of each channel and drying takes place at $20 \text{ }^\circ\text{C}$ and 80% humidity. In whole soil experiments, there is a much greater surface area relative to the volume and drying takes place at $40 \text{ }^\circ\text{C}$ and 0% humidity. The smaller interfacial area and the lower external evaporativity lead to greater sensitivity and slower evaporation in the micromodels.

Surprisingly, we observed no difference in water content in bacterial colony samples collected from agar plates across treatments of EPS+ and EPS- strains of *S. meliloti*. The fact that evaporation resistance is only seen in a micro-structured setting (soil or micro), and not in a pure bacterial colony samples suggests a synergistic effect of physical microstructure and chemical features of the biological sample in evaporation resistance.

We hypothesize that hydrophilic solid surfaces may provide mechanical stability for a dry and denser interface formed at the edges of the collapsing EPS matrix with evaporation (Roberson et al., 1993). This crust has an intrinsically lower permeability to water, but without mechanical stabilization, cracks may form, thus exposing the EPS interior. Cracking of the EPS matrix under desiccation has been observed by microscopy in EPS-amended soils (Chenu, 1993). To test this hypothesis, additional experiments are needed to test permeability and mechanical properties of model hydrogel membranes in various physically confined and supported geometries.

Table 2
Drying times for each microchannel.

Channel	EPS+ drying time (h)	EPS- drying time (h)	Difference (h)	Ratio (EPS+ drying time/EPS- drying time)
1	24.0	13.5	10.5	1.8
2	24.5	12.0	12.5	2.0
3	25.5	11.5	14.0	2.2
4	24.5	11.5	13.0	2.1
5	19.0	7.5	11.5	2.5
6	18.5	16.5	2.0	1.1
Average	23	12	11	1.9

4.2. Water evaporation rate and implications for agriculture

We provide direct evidence that microbes can modulate water evaporation at the pore scale. The average wilting point for many crops is commonly assumed to be -15 bar (-1.5 MPa), or between 15 and 27% volumetric water content (Powers, 1922). Here, micromodels filled with the EPS– bacterial suspension dropped below 15% volumetric water content at about 8.5 h. This corresponds to 27% saturation (Fig. 5A), with saturation defined as volumetric water content divided by micromodel porosity, here 57%. Meanwhile, physically identical micromodels filled with the EPS+ bacterial suspension were still at 32% water content (55% saturation) at 8.5 h. A slower rate of water loss is the key difference between EPS+ and EPS– treatments.

The rate of water loss may have important implications for agriculture. Global circulation models do not necessarily predict changes in the amount of precipitation in many areas, but the rain that comes will be associated with more extreme events separated by longer rain return intervals (Field et al., 2012). Changing precipitation patterns may result in reduced soil moisture in many regions. Sandhya et al. (2009) and Alami et al. (2000) showed amending soil with bacteria that produce EPS has the potential to slow evaporation. In combination with EPS-mediated soil structuring (Amellal et al., 1998; Emerson and McGarry, 2003), the drying resistance effects demonstrated here could translate into field-scale effects over weather event-relevant timescales.

4.3. Extensions and limitations

Emulated soil micromodels allow systematic replication or alteration of micro-scale physical geometry. Although physical features can be controlled, variability in bacterial responses may lead to slight variations in overall performance of the bio-physico-chemical system. Fortunately, photolithography and soft lithography approaches are well-adapted to high-throughput analysis with identical physical structures used for multiple replicates across treatments.

The experiments described here employed a single physical geometry. However, our techniques are amenable to systematic alteration of physical pore geometry. The spatial arrangement of the simulated soil grains can be altered to create aggregated and non-aggregated variations. Such experiments would help determine the relative importance of physical geometry versus solution chemistry in microbially-mediated pore-scale evaporation resistance.

Our micromodels feature a complex 2-D physical geometry, a uniform solid phase chemistry (a surface-treated polymer, not geological material), and an initially uniform solution chemistry. Clearly, this approach cannot capture all the physical, chemical, or biological features of real soils such as heterogeneous surface chemistry, steep micro-scale gradients in solution composition, and a patchy distribution of microorganisms. In particular, plant exudates in the rhizosphere have been shown to support a microhabitat with drastically different properties than bulk soil. Microfluidic devices have been used to examine responses of bacterial biofilms to chemical gradients (Deng et al., 2013). Ever more complex micromodels could be developed that also incorporate other important features of the soil system, such as micro-scale gradients of plant exudates, to probe the effect of localized chemical conditions on microbial EPS production and pore-scale water retention near plant roots.

Finally, the minimum pore throat spacing in the emulated soil micromodels described here is about $5\ \mu\text{m}$. Pore spaces smaller than $5\ \mu\text{m}$ are common in soils. Other microfabrication techniques could be used to create physical features down to about $1\ \mu\text{m}$,

provided a commensurate reduction in the depth of the microchannels is also implemented. However, photolithography cannot be used to pattern features smaller than the wavelength of ultraviolet light. Other techniques including electron beam lithography can achieve greater resolution, but with potentially unacceptable costs and limitations in terms of materials, time, and a reduction in the device footprint.

5. Conclusions

Here we demonstrate the use of emulated soil micromodels to better understand how microbial processes modulate water availability at the pore scale. We provide direct evidence that microbial activities alter water retention at the pore scale. The mechanism proposed for pore-scale moisture retention is a physical stabilization of the polymeric skin at the air–water interface in the EPS+ treatment. Additional work will be needed to test the proposed mechanism and to provide greater predictive capability of microbial-mediated moisture retention in real soils.

Emulated soil micromodels are synthetic, idealized experimental systems. Micromodels are not meant to replace experiments performed with real soils or field-scale investigations. Rather, they provide a systematic approach for building pore-scale understanding of the physical, chemical, and biological factors that interact in real soils. By using emulated soil micromodels, pore-scale geometry can be exactly replicated. Geometrically defined micro-scale systems can greatly increase the sensitivity of water loss measurement compared to standard approaches. Additional features of real soils can be incorporated into micromodels of increasing complexity.

As a starting point, the micromodel approach described here may be useful in developing sustainable agriculture biotechnologies. By holding physical geometry and external evaporativity constant, the technique could be used to screen the ability of different microbial strains to produce EPS under various conditions for the purpose of controlling soil moisture. One day, it may be possible to more sustainably retain soil moisture by stimulating natural microbial processes *in situ*.

Acknowledgments

This work was supported by USDA NIFA-AFRI awards 2012-67020-19380 and 2012-67014-30232 and NSF awards 1137249 and 1027125. Additional thanks are extended to Dr. Laura Pinatti, Dr. Ekneet Shani, Mr. Jonathan Drasdis and Dr. Lokesh Kumar for the aid they provided throughout.

Appendix A. Supplementary data

Supplementary data related to this article can be found at <http://dx.doi.org/10.1016/j.soilbio.2014.12.006>.

References

- Addae-Mensah, K.A., Retterer, S., Opalenik, S.R., Thomas, D., Lavrik, N.V., Wikswo, J.P., 2009. Cryogenic etching of silicon: an alternative method for fabrication of vertical microcantilever master molds. *Journal of Microelectromechanical Systems* 19.
- Alami, Y., Achouak, W., Marol, C., Heulin, T., 2000. Rhizosphere soil aggregation and plant growth promotion of sunflowers by an exopolysaccharide-producing *Rhizobium* sp. strain isolated from sunflower roots. *Applied and Environmental Microbiology* 66, 3393–3398.
- Amellal, N., Burtin, G., Bartoli, F., Heulin, T., 1998. Colonization of wheat roots by an exopolysaccharide-Producing *Pantoea* agglomerans strain and its effect on rhizosphere. *Soil Aggregation* 64, 10.
- Bouchillon, G.M., Chau, J.F., McManus, G.B., Shor, L.M., 2014. Microfluidic passive samplers for *in situ* collection of live aquatic protists. *Analytical Methods* 6, 8350–8357.

- Carminati, A., Schneider, C.L., Moradi, A.B., Zarebanadkouki, M., Vetterlein, D., Vogel, H.-J., Hildebrandt, A., Weller, U., Schüler, L., Oswald, S.E., 2011. How the rhizosphere may favor water availability to roots. *Vadose Zone Journal* 10, 988–998.
- Chau, J.F., Bagtzoglou, A.C., Willig, M.R., 2011. The effect of soil texture on richness and diversity of bacterial communities. *Environmental Forensics* 12, 333–341.
- Chau, J.F., Or, D., 2006. Linking drainage front morphology with gaseous diffusion in unsaturated porous media: a lattice Boltzmann study. *Physical Review E – Statistical, Nonlinear, and Soft Matter Physics* 74.
- Chau, J.F., Or, D., Sukop, M.G., 2005. Simulation of gaseous diffusion in partially saturated porous media under variable gravity with lattice Boltzmann methods. *Water Resources Research* 41, 1–11.
- Chenu, C., 1993. Clay- or sand-polysaccharide associations as models for the interface between micro-organisms and soil: water related properties and microstructure. *Geoderma* 56, 143–156.
- Chenu, C., Roberson, E.B., 1996. Diffusion of glucose in microbial extracellular polysaccharide as affected by water potential. *Soil Biology & Biochemistry* 28, 877–884.
- Cho, G.-C., Dodds, J., Santamaria, J.C., 2006. Particle shape effects on packing density, stiffness, and strength: natural and crushed sands. *Journal of Geotechnical and Geoenvironmental Engineering* 132, 591–602.
- Cho, H.J., Jonsson, H., Campbell, K., Melke, P., Williams, J.W., Jedynak, B., Stevens, A.M., Groisman, A., Levchenko, A., 2007. Self-organization in high-density bacterial colonies: efficient crowd control. *Plos Biology* 5, 2614–2623.
- Dai, A., 2011. Drought under global warming: a review. *Wiley Interdisciplinary Reviews: Climate Change* 2, 45–65.
- Dechesne, A., Wang, G., Gülez, G., Or, D., Smets, B.F., Tiedje, J.M., 2010. Hydration-controlled bacterial motility and dispersal on surfaces. *Proceedings of the National Academy of Sciences of the United States of America* 107, 14369–14372.
- Deng, J., Dhummakupt, A., Samson, P.C., Wikswo, J.P., Shor, L.M., 2013. Dynamic dosing assay relating real-time respiration responses of *Staphylococcus aureus* biofilms to changing microchemical conditions. *Analytical Chemistry* 85, 5411–5419.
- Emerson, W.W., McGarry, D., 2003. Organic carbon and soil porosity. *Australian Journal of Soil Research* 41, 107–118.
- Field, C.B., Barros, V., Stocker, T.F., Dahe, Q., 2012. Managing the Risks of Extreme Events and Disasters to Advance Climate Change Adaptation: Special Report of the Intergovernmental Panel on Climate Change. Cambridge University Press.
- Flemming, H.-C., 2011. The perfect slime. *Colloids and Surfaces B: Biointerfaces* 86, 251–259.
- Friedman, S.P., Robinson, D.A., 2002. Particle shape characterization using angle of repose measurements for predicting the effective permittivity and electrical conductivity of saturated granular media. *Water Resources Research* 38, 1236.
- Gage, D.J., 2004. Infection and invasion of roots by symbiotic, nitrogen-fixing rhizobia during nodulation of temperate legumes. *Microbiology and Molecular Biology Reviews* 68, 280–300.
- Gajic, B., Durovic, N., Dugalic, G., 2010. Composition and stability of soil aggregates in fluviosols under forest, meadows, and 100 years of conventional tillage. *Journal of Plant Nutrition and Soil Science* 173, 502–509.
- Galibert, F., Finan, T.M., Long, S.R., Puhler, A., Abola, P., et al., 2001. The composite genome of the legume symbiont *Sinorhizobium meliloti*. *Science* 293, 668–672.
- Jia, X., Williams, R.A., 2001. A packing algorithm for particles of arbitrary shapes. *Powder Technology* 120, 175–186.
- Kets, E.P.W., deBont, J.A.M., Heijpeper, H.J., 1996. Physiological response of *Pseudomonas putida* S12 subjected to reduced water activity. *Fems Microbiology Letters* 139, 133–137.
- Kim, H.J., Boedicker, J.Q., Choi, J.W., Ismagilov, R.F., 2008. Defined spatial structure stabilizes a synthetic multispecies bacterial community. *Proceedings of the National Academy of Sciences* 105, 18188–18193.
- Langelier, S.M., Livak-Dahl, E., Manzo, A.J., Johnson, B.N., Walter, N.G., Burns, M.A., 2011. Flexible casting of modular self-aligning microfluidic assembly blocks. *Lab Chip* 11, 1679–1687.
- Lanning, L.M., Ford, R.M., Long, T., 2008. Bacterial chemotaxis transverse to axial flow in a microfluidic channel. *Biotechnology and Bioengineering* 100, 653–663.
- Li, X., Yuan, Y., 2002. Settling velocities and permeabilities of microbial aggregates. *Water Research* 36, 3110–3120.
- Long, T., Ford, R.M., 2009. Enhanced transverse migration of bacteria by chemotaxis in a porous T-sensor. *Environmental Science & Technology* 43, 1546–1552.
- Long, T., Or, D., 2009. Dynamics of microbial growth and coexistence on variably saturated rough surfaces. *Microbial Ecology* 58, 262–275.
- Mao, H., Cremer, P.S., Manson, M.D., 2003. A sensitive, versatile microfluidic assay for bacterial chemotaxis. *Proceedings of the National Academy of Sciences* 100, 5449–5454.
- Markov, D.A., Samson, P.C., Schaffer, D.K., Dhummakupt, A., Wikswo, J.P., Shor, L.M., 2010. Window on a microworld: simple microfluidic systems for studying microbial transport in porous media. *Journal of Visualized Experiments* 39.
- Matz, C., Kjelleberg, S., 2005. Off the hook – how bacteria survive protozoan grazing. *Trends in Microbiology* 13, 302–307.
- Morales, V.L., Parlange, J.Y., Steenhuis, T.S., 2010. Are preferential flow paths perpetuated by microbial activity in the soil matrix? A review. *Journal of Hydrology* 393, 29–36.
- Moyano, F.E., Manzoni, S., Chenu, C., 2013. Responses of soil heterotrophic respiration to moisture availability: an exploration of processes and models. *Soil Biology and Biochemistry* 59, 72–85.
- Mueller, K., Gonzalez, J.E., 2011. Complex regulation of symbiotic functions is coordinated by MucR and quorum sensing in *Sinorhizobium meliloti*. *Journal of Bacteriology* 193, 485–496.
- Mukhopadhyay, R., 2007. When PDMS isn't the best. *Analytical Chemistry* 79, 3248–3253.
- Or, D., Phutane, S., Dechesne, A., 2007a. Extracellular polymeric substances affecting pore-scale hydrologic conditions for bacterial activity in unsaturated soils. *Vadose Zone Journal* 6, 298–305.
- Or, D., Smets, B.F., Wraith, J.M., Dechesne, A., Friedman, S.P., 2007b. Physical constraints affecting bacterial habitats and activity in unsaturated porous media – a review. *Advances in Water Resources* 30, 1505–1527.
- Or, D., Wraith, J.M., 2002. Soil water content and water potential relationships. In: Warrick, A. (Ed.), *Soil Physics Companion*. CRC Press, Boca Raton, pp. 49–84.
- Park, E.-J., Sul, W.J., Smucker, A.J., 2007. Glucose additions to aggregates subjected to drying/wetting cycles promote carbon sequestration and aggregate stability. *Soil Biology and Biochemistry* 39, 2758–2768.
- Pellock, B.J., Teplitski, M., Boinay, R.P., Bauer, W.D., Walker, G.C., 2002. A LuxR homologue controls production of symbiotically active extracellular polysaccharide II by *Sinorhizobium meliloti*. *Journal of Bacteriology* 184, 5067–5076.
- Potts, M., 1994. Desiccation tolerance of prokaryotes. *Microbiological Reviews* 58, 755–805.
- Powers, W.L., 1922. Field structure capacity and wilting point of soils. *Soil Science* 14, 159–166.
- Ramos, C., Licht, T.R., Sternberg, C., Krogfelt, K.A., Molin, S., 2001. Monitoring bacterial growth activity in biofilms from laboratory flow chambers, plant rhizosphere, and animal intestine. *Microbial Growth in Biofilms*, Pt B 21–42.
- Rinaudi, L.V., Gonzalez, J.E., 2009. The low-molecular-weight fraction of exopolysaccharide II from *Sinorhizobium meliloti* is a crucial determinant of biofilm formation. *Journal of Bacteriology* 191, 7216–7224.
- Roberson, E.B., Chenu, C., Firestone, M.K., 1993. Microstructural changes in bacterial exopolysaccharides during desiccation. *Soil Biology and Biochemistry* 25, 1299–1301.
- Roberson, E.B., Firestone, M.K., 1992. Relationship between desiccation and exopolysaccharide production in a soil *Pseudomonas* sp. *Applied and Environmental Microbiology* 58, 1284–1291.
- Roman, G.T., Culbertson, C.T., 2006. Surface engineering of poly(dimethylsiloxane) microfluidic devices using transition metal sol–gel chemistry. *Langmuir* 22, 4445–4451.
- Sandhya, V., Grover, M., Reddy, G., Venkateswarlu, B., 2009. Alleviation of drought stress effects in sunflower seedlings by the exopolysaccharides producing *Pseudomonas putida* strain GAP-P45. *Biology and Fertility of Soils* 46, 17–26.
- Sauer, K., Camper, A.K., Ehrlich, G.D., Costerton, J.W., Davies, D.G., 2002. *Pseudomonas aeruginosa* displays multiple phenotypes during development as a biofilm. *Journal of Bacteriology* 184, 1140–1154.
- Schindelin, J., Arganda-Carreras, I., Frise, E., Kaynig, V., Longair, M., Pietzsch, T., Preibisch, S., Rueden, C., Saalfeld, S., Schmid, B., Tinevez, J.Y., White, D.J., Hartenstein, V., Eliceiri, K., Tomancak, P., Cardona, A., 2012. Fiji: an open-source platform for biological-image analysis. *Nature Methods* 9, 676–682.
- Scholl, M.A., Mills, A.L., Herman, J.S., Hornberger, G.M., 1990. The influence of mineralogy and solution chemistry on the attachment of bacteria to representative aquifer materials. *Journal of Contaminant Hydrology* 4, 321–326.
- Schulte, E.E., Hopkins, B.G., 1996. Estimation of soil organic matter by weight loss-on-ignition. *Soil Science Society of America* 46, 21–31.
- Singh, R., Olson, M.S., 2011. Transverse mixing enhancement due to bacterial random motility in porous microfluidic devices. *Environmental Science & Technology* 45, 8780–8787.
- Steinhaus, B., Garcia, M.L., Shen, A.Q., Angenent, L.T., 2007. A portable anaerobic microreactor reveals optimum growth conditions for the methanogen *Methanoseta concilii*. *Applied and Environmental Microbiology* 73, 1653–1658.
- Sukop, M.C., Or, D., 2003. Invasion percolation of single component, multiphase fluids with lattice Boltzmann models. *Physica B* 338, 298–303.
- Wang, G., Or, D., 2010. Aqueous films limit bacterial cell motility and colony expansion on partially saturated rough surfaces. *Environmental Microbiology* 12, 1363–1373.
- Wang, G., Or, D., 2013. Hydration dynamics promote bacterial coexistence on rough surfaces. *ISME Journal* 7, 395–404.
- Wang, W., Shor, L.M., LeBoeuf, E.J., Wikswo, J.P., Kosson, D.S., 2005. Mobility of protozoa through narrow channels. *Applied and Environmental Microbiology* 71 (8), 4628–4637.
- Wang, W., Shor, L.M., LeBoeuf, E.J., Wikswo, J.P., Taghon, G.L., Kosson, D.S., 2008. Protozoa migration in Bent microfluidic channels. *Applied and Environmental Microbiology* 74, 1945–1949.
- Weibel, D.B., DiLuzio, W.R., Whitesides, G.M., 2007. Microfabrication meets microbiology. *Nature Reviews Microbiology* 5, 209–218.
- Whitesides, G., Ostuni, E., Takayama, S., Jiang, X., Ingber, D., 2001. Soft lithography in biology and biochemistry. *Annual Review of Biomedical Engineering* 3, 335–373.
- Young, I.M., Crawford, J.W., 2004. Interactions and self-organization in the soil-microbe complex. *Science* 304, 1634–1637.